ACS APPLIED MATERIALS & INTERFACES

Research Article

www.acsami.org

Fabrication of High-Surface-Area Graphene/Polyaniline Nanocomposites and Their Application in Supercapacitors

Zhe-Fei Li,[†] Hangyu Zhang,[‡] Qi Liu,[†] Lili Sun,[†] Lia Stanciu,[‡,§] and Jian Xie*,[†]

[†]Department of Mechanical Engineering, Purdue School of Engineering and Technology, Indiana University-Purdue University (IUPUI), Indianapolis, Indiana 46202, United States

[‡]Weldon School of Biomedical Engineering, Purdue University, West Lafayette, Indiana, 47907, United States

[§]School of Materials Engineering, Purdue University, West Lafayette, Indiana, 47907, United States

Supporting Information

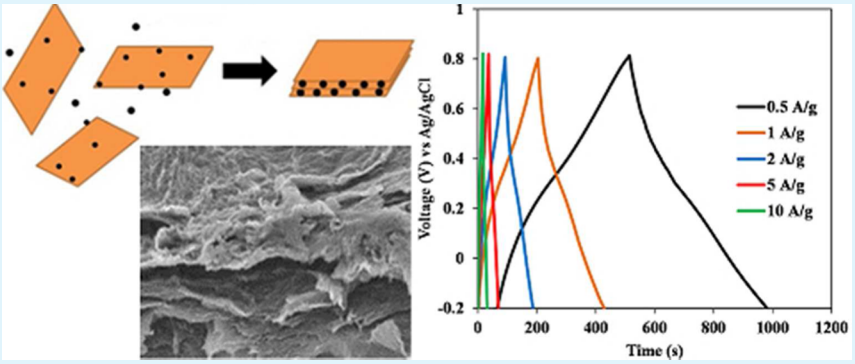

ABSTRACT: Graphene/polyaniline (PANI) nanocomposites were prepared by reducing graphene oxide with hydrazine in the presence of different amounts of polyaniline nanoparticles. In situ cryo-transmission electron microscope (TEM) images of a graphene oxide (GO)/PANI solution revealed that the PANI nanoparticles were anchored on the surface of the GO sheets. During the reduction, the as-adsorbed PANI nanoparticles were sandwiched between layers of graphene sheets. These PANI nanoparticles acted as spacers to create gaps between neighboring graphene sheets, resulting in a higher surface area compared to pure graphene. Graphene/PANI nanocomposites exhibited the high specific surface area of 891 m^2/g. Utilizing this composite material, a supercapacitor with a specific capacitance of 257 F/g at a current density of 0.1 A/g has been achieved.

KEYWORDS: *graphene, polyaniline, nanocomposites, N_2 adsorption isotherm, supercapacitor*

1. INTRODUCTION

Since the first isolation and observation of single-layer graphene by Novoselov et al. in 2004, graphene has attracted tremendous research interest.[1] Graphene is a single-atom-thick, two-dimensional sheet of sp^2-hybrized carbon atoms arranged in a honeycomb crystal structure with exceptionally high strength, surface area, thermal conductivity, and electronic conductivity.[2,3] These superior properties make graphene a very promising candidate in many applications, such as sensors,[4] field-effect-transistors,[5] gas sorbents,[6] fuel cells,[7] batteries,[8,9] and supercapacitors.[10−12] Graphene has been prepared by several methods, such as mechanical exfoliation,[13] direct growth from organic precursors,[14] epitaxial growth on SiC,[15] chemical vapor deposition,[16,17] and chemical exfoliation. Among these methods, chemical exfoliation has been the most employed method to fabricate graphene-based devices due to its advantages of facile aqueous synthesis, low cost, and easy scale up.[10,18−20]

While extremely promising, present graphene-based devices have not shown performance as high as those theoretically predicted. This is mainly caused by the relatively low surface area of chemically produced graphene. Generally, graphene is yielded by the chemical reduction of graphene oxide (GO). GO is a layered stack of oxidized graphene sheets with different functional groups and can be completely exfoliated upon the addition of mechanical energy. The exfoliation is accomplished due to the hydrophilicity of the oxygen-containing (i.e., epoxide and hydroxyl) functionalities introduced during the oxidation of the graphite. Thus, GO can be easily dispersed into single sheets in water at low concentrations (less than 1 mg/mL). However, upon the removal of the hydrophilic functional groups on the GO, the reduced GO sheets were inclined to restack, leading to aggregated graphene sheets a few layers thick.[21] This restacking resulted in a significant decrease in the surface area of the graphene, consequently leading to poor performance. Therefore, the creation of high-surface-area graphene is of paramount significance to advance the applications of graphene.

Received: January 14, 2013
Accepted: March 12, 2013
Published: March 12, 2013

Adhering nanoparticles onto the graphene surface before graphene sheet restacking occurs is an effective way to maintain the high surface area of graphene. Various nanoparticles have been reported to prevent the aggregation of graphene sheets. Anchoring RuO_2 on the graphene surface increased the surface area from 108 to 281 m^2/g.[22] Si and Samulski deposited Pt nanoparticles on graphene surfaces before drying, and the surface area of the resulting composite was as high as 862 m^2/g.[23] Yan et al. reported the use of acetylene black to inhibit the agglomeration of graphene, and the surface area of the resulting composites was 586 m^2/g.[24] However, the resulting specific surface area was still lower than the theoretical surface area of a single graphene layer (2630 m^2/g). This could be due to poor adhesion of spacers to graphene. Therefore, nanoparticles that can strongly adsorb onto graphene will be of great importance to achieve graphene with a surface area approaching the theoretical value.

In the present work, graphene/polyaniline (PANI) nanoparticle composites were prepared by reducing GO in the presence of different contents of PANI nanoparticles. PANI is a conducting polymer that contains positively charged amine/imine groups on its polymer chain, which may favor adhesion onto the GO surface. A schematic illustration of this procedure is shown in Figure 1. Our results showed that the use of PANI

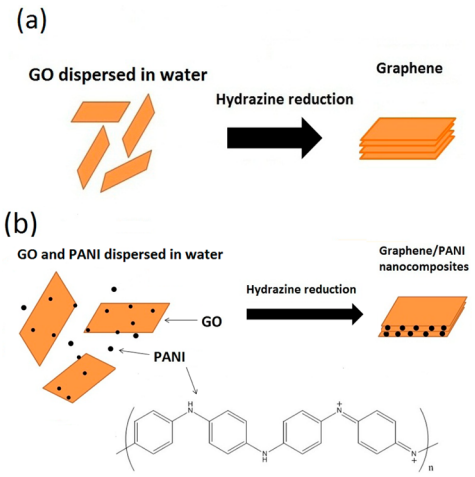

Figure 1. Schematic illustration of the preparation of (a) graphene and (b) graphene/PANI nanocomposites.

as the spacer can partially prevent graphene sheets from restacking, resulting in an increase in the specific surface area. Graphene nanocomposites with 2 wt % PANI (ratio to GO) exhibited a high specific surface area of 891 m^2/g and a mesoporous structure. The high surface area and the mesoporous structure of the prepared composites allow faster transport by electrolyte ions, consequently leading to excellent performance as supercapacitors.

2. EXPERIMENTAL SECTION

2.1. Synthesis of GO. The GO was prepared using a modified Hummer's method.[25,26] Prior to the Hummer's method, an additional graphite oxidation procedure was carried out. Two grams of graphite flakes was mixed with 10 mL of concentrated H_2SO_4, 2 g of $(NH_4)_2S_2O_8$, and 2 g of P_2O_5. The resulting mixture was stirred constantly and heated at 80 °C for 4 h. The mixture was then filtered and washed with DI water. The product was dried in an oven at 80 °C overnight. This preoxidized graphite was then subjected to oxidation by the Hummers' method. Two grams of preoxidized graphite, 1 g of sodium nitrate, and 46 mL of sulfuric acid were mixed and stirred for 15 min in a 500 mL flask immersed in an ice bath. Then, 6 g of potassium permanganate was slowly added to the above suspension solution and cooled for another 15 min. Water (92 mL) was added slowly to the suspension, causing a violent effervescence. The temperature was maintained at about 98 °C for 15 min. The suspension was diluted by 280 mL of warm water and treated with 10 mL of 30% H_2O_2 to reduce the unreacted permanganate. Finally, the resulting suspension was centrifuged at 12 000 rpm a few times to remove residual salts and acid. The purified GO was dispersed in DI water at a concentration of 0.2 mg/mL and sonicated for 1 h. Then, the GO dispersion was subjected to another centrifugation at 5000 rpm for 5 min to remove the unexfoliated GO. The resulting GO colloid solution is able to remain stable for a few months.

2.2. Synthesis of PANI. The PANI nanoparticles were synthesized by chemical oxidative polymerization in the presence of HCl and poly(4-styrenesulfonate) (PSS).[27] Aniline monomer, 0.53 mmol, was dissolved in 40 mL of 0.5 M aqueous HCl solution. Then, 0.6 g of aqueous PSS solution was added to the above solution and was stirred for 1 h. The polymerization of aniline was conducted by adding 0.69 mmol of ammonium persulfate as an oxidizing agent for 12 h at room temperature. After polymerization, PANI nanoparticles were collected by filtration and freeze-dried.

2.3. Synthesis of Graphene and Graphene/PANI Nanocomposites. Graphene/PANI composites with different PANI content (wt % of GO) were prepared by reducing the mixture of the graphene oxide dispersion with the anchored highly hydrophilic PANI. The PANI aqueous dispersion was added to 200 mL of the GO solution. The mixture was stirred for 1 h and then subjected to sonication for 1 h. Subsequently, a hydrazine solution was added into the mixture, and the mixture was stirred and heat treated at 90 °C for 24 h. Then, the mixture was filtered by a 0.025 μm membrane, washed with DI water, and freeze-dried.

2.4. Fabrication of Supercapacitor Electrodes. The supercapacitor electrode was prepared by casting a Nafion-impregnated sample onto a glassy carbon electrode with a diameter of 5 mm. The electrode material (5 mg) was first dispersed by sonication for 1 h in 5 mL of ethanol/water mixture (1:4 v/v) containing 10 μL of Nafion solution (5 wt % in water, Ion Power, Inc.). This dispersion (10 μL) was then dropped onto the glassy carbon electrode and dried at 80 °C before electrochemical testing.

2.5. Characterization. The morphology of the graphene and the graphene/PANI nanocomposites was characterized by a Philips CM 200 transmission electron microscope (TEM) and an FEI NOVA field-emission scanning electron microscope (FE-SEM). For cryogenic TEM (cryo-TEM) analysis, 3.5 μL of the sample was dropped onto a copper grid coated with holey carbon film. The grid was immediately plunged into liquid ethane cooled by liquid N_2. The sample grid was then loaded into the microscope with a Gatan side-entry cryo-holder. Cryo-TEM images were collected using the Philips CM200 with a field emission gun operating at 200 kV. The specific surface areas of the graphene, the PANI, and the nanocomposites were determined by the Brunauer–Emmett–Teller (BET) method of nitrogen sorption at 77 K using a Quantachrome Autosorb-1 surface area analyzer. The pore size distribution was calculated using a NLDFT model, assuming cylindrical slit-shaped pore geometry for the pores. The structural and compositional information of the graphene, the PANI, and the composites were analyzed using a Kratos AXIS Ultra X-ray photoelectron spectrometer (XPS).

2.6. Electrochemical Measurements. A three-electrode cell system was used to evaluate electrochemical performance using cyclic voltammetry (CV), galvanostatic charge/discharge, and electrochemical impedance spectroscopy (EIS) using a Solartron 1287 electrochemical workstation. An aqueous solution of 1 M H_2SO_4 was used as the electrolyte. A platinum sheet and a saturated Ag/AgCl electrode were used as the counter and the reference electrode, respectively. CV curves were measured between −0.2 and 0.8 V vs Ag/AgCl at different scan rates. Galvanostatic charge/discharge tests were performed at current densities of 0.1, 0.3, 0.5, 1, 2, 5, and 10 A/g. EIS measurement was carried out at open circuit potential with AC

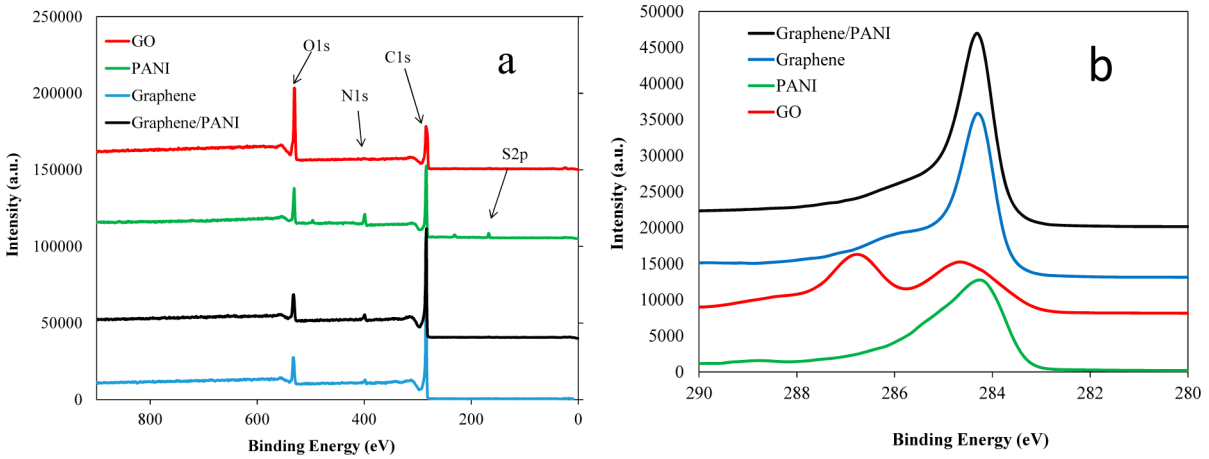

Figure 2. (a) XPS spectra and (b) high resolution C 1s spectra of of the PANI, graphene oxides, graphene, and graphene/PANI composites.

amplitude of 5 mV over the frequency range from 100 kHz to 0.1 Hz. The specific gravimetric capacitance was calculated from the discharge process according to the following equation:

$$C = \frac{I\Delta t}{m\Delta V} \quad (1)$$

where C is the specific capacitance of the active material (F/g), I is the applied current (A), Δt is the total discharge time (s), ΔV is the potential change (V), and m is the mass of active material (g) in the electrode.

3. RESULTS AND DISCUSSION

3.1. Composition Analysis. The atomic composition of the GO, graphene, PANI, and graphene/PANI composites was analyzed by XPS, and the comparative results are shown in Figure 2 and Tables 1 and 2. The C/O ratio in Table 1 is an indication of the oxygen-containing functional groups (i.e., C−O, C═O, C(O)O). The C/O ratio of GO (2.4) is much lower than that of the graphene (10.9) and the graphene/PANI nanocomposites (11.3), suggesting that the functional groups on the surface of the GO were mostly reduced. It can be seen in Table 1 that PANI has a higher N and S composition than graphene-based materials. Compared with pure graphene, the higher N and S content in graphene/PANI composites probably indicates the presence of PANI in graphene/PANI composites. The nitrogen content in graphene sample may be incorporated through the reaction of hydrazine with the carbonyl groups of GO.[28,29] The curve fitting of C 1s spectra were performed and shown in Figure S1, Supporting Information. The detailed functional groups on the surfaces of GO, graphene, PANI, and graphene/PANI composites are listed in Table 2. Similar to the C/O ratio, the relative ratio of oxygen-containing functional groups in graphene and graphene/PANI are much smaller than those of GO, which is consistent with other findings.[28,30,31] Upon hydrazine reduction, the relative ratio of C−O and C═O functional groups is significantly reduced.

Table 1. Elemental Composition of GO, Graphene, PANI, and Graphene/PANI Composites[a]

sample	C (%)	O (%)	N (%)	S (%)	C:O
GO	69.8	29.1	0	0.08	2.4
graphene	90.5	8.3	1.6	0.03	10.9
PANI	79.3	11.7	6.9	2.06	6.7
graphene/PANI	89.6	7.9	2.34	0.13	11.3

[a]In atomic percent.

3.2. N_2 Adsorption Isotherm, BET Surface Area, and Pore Size Distribution. To study the effects of PANI on preventing the restacking of graphene, N_2 adsorption−desorption isotherms were measured by a Quantachrome Autosorb-1 surface area analyzer at 77 K. The N_2 adsorption−desorption isotherms and the pore size distribution of the as-prepared composites with different PANI content are shown in Figure 3. The N_2 adsorption−desorption isotherms (Figure 4a) show that graphene materials possess a Type IV isotherm and a Type H3 hysteresis loop (according to the International Union of Pure and Applied Chemistry (IUPAC) classification), indicating the presence of mainly mesoporous structure and slit-shaped pores.[32,33] Therefore, the pore size distribution (Figure 4b) was obtained by a hybrid DFT (NLDFT) model, assuming cylindrical slit-shaped pore geometry for the mesopores.[34] With the addition of PANI, both the N_2 adsorption amount and the pore volume of the graphene/PANI composites were higher than those of graphene without PANI. It was revealed that the pore size distribution center was at about 5 nm for all the graphene samples. The amount of mesopores around 3−6 nm and micropores of 1−2 nm was

Table 2. Relative Ratio (%) of Different Carbon Components in GO, Graphene, and Graphene/PANI Composites from C 1s XPS Spectra

sample	C═C	C−C	C−N/C−S	C−O	C═O	C(O)O
binding energy (eV)	284.3	285.0	285.8	286.6	287.8	289.3
GO	24.3	22.4	5.1	32.1	9.1	4.5
graphene	43.7	21.0	7.3	6.4	5.8	3.2
graphene/PANI	44.5	20.5	8.9	5.1	5.7	3.3
PANI	71.3 (C−C)		16.9 (C═N)		7.5 (C═N+)	3.8 (C−S)

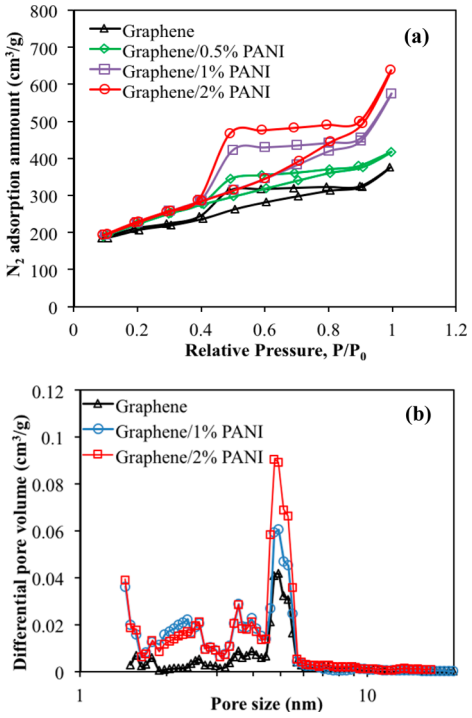

Figure 3. (a) Nitrogen adsorption and desorption isotherms and (b) pore size distribution of the as-prepared composites with different PANI contents.

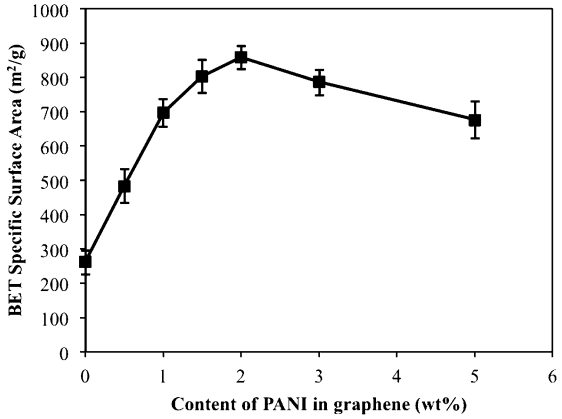

Figure 4. Effects of PANI content on the BET specific surface area of the graphene/PANI composites.

also increased with the incorporation of the PANI into the graphene. The pore volume of all samples is displayed in Table S1 (Supporting Information).

The specific surface area of graphene and its composites was calculated on the basis of BET theory and is shown in Figure 4. It can be noticed that the BET specific surface area of the graphene without the addition of PANI was only 268 m^2/g. As the PANI content in the composites was increased, the specific surface area of the resulting composites also increased, peaking at around 2 wt % PANI content, and then decreased. A high BET specific surface area of the composites with 2 wt % PANI was determined to be as high as 891 m^2/g, which is much higher than that of either the PANI (49 m^2/g) or the pure graphene (268 m^2/g). This large specific surface area of graphene/PANI suggests that the introduction of PANI nanoparticles between the 2D graphene sheets can reduce the layer-to-layer stacking, when compared to that of pure graphene. When the PANI content is equal to 3% or higher, the BET surface area of the resulting composites decreases slightly, though it is still significantly higher than that of pure graphene. This slight decrease could be attributed to the relatively low surface area of PANI (49 m^2/g). Another possibility is that the PANI nanoparticles may aggregate at higher concentration, consequently limiting their influence on reducing graphene restacking.

3.3. Morphology of Graphene and Graphene/PANI Composites. PANI/PSS nanoparticles were synthesized via a chemical oxidative polymerization of aniline with PSS as the dopant and stabilizer.[27,35] Figure S2, Supporting Information, shows the SEM image of PANI/PSS nanoparticles, which possessed a particle-size distribution of mainly 20−40 nm. Graphene/PANI nanocomposites were prepared by in situ chemical reduction of exfoliated GO in the presence of different amounts of PANI. As shown in Figure 1b, the synthesis consists of three steps: (1) the exfoliation of GO in a diluted aqueous solution; (2) the uniform mixing of GO and PANI; (3) the chemical reduction by hydrazine. The morphology of GO, graphene, and graphene/PANI composites was studied by SEM and TEM, as shown in Figures 5 and 6. A layered structure has

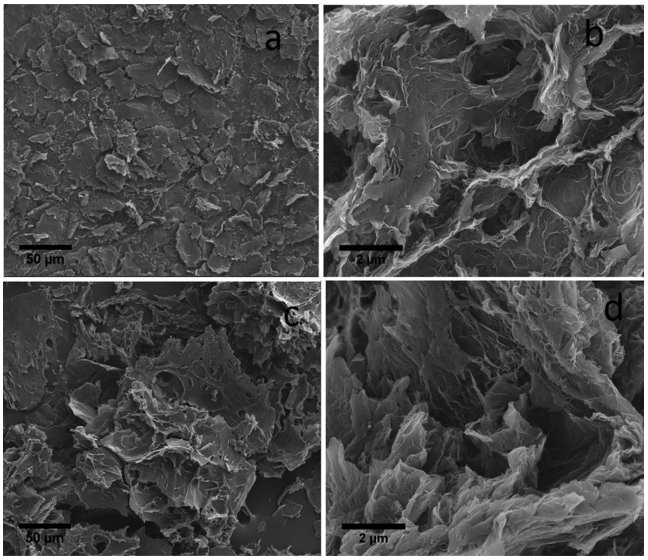

Figure 5. SEM image of (a) low magnification and (b) high magnification of pure graphene and (c) low magnification and (d) high magnification of graphene/PANI nanocomposites.

been observed in SEM images of both pure graphene (Figure 5a,b) and graphene/PANI composites (Figure 5c,d), which results from the stacking of the graphene sheets because of the van der Waals force interaction. In order to study the influence of the addition of PANI in preventing graphene restacking, cryo-TEM was utilized to study the morphology of GO and PANI in aqueous solutions. The cryo-TEM technique can be used to image a sample frozen in an aqueous solution by liquid N_2, which does not alter its original morphology during the sample preparation. It is shown in Figure 6a that, upon mixing the GO and the PANI in the solution, some of PANI particles were adsorbed on the GO sheet (as pointed out by the arrows). The TEM image of the freeze-dried GO solution with 2 wt % PANI before the hydrazine reduction (Figure 6b) also indicates that the PANI particles tend to adsorb on the GO sheet. After

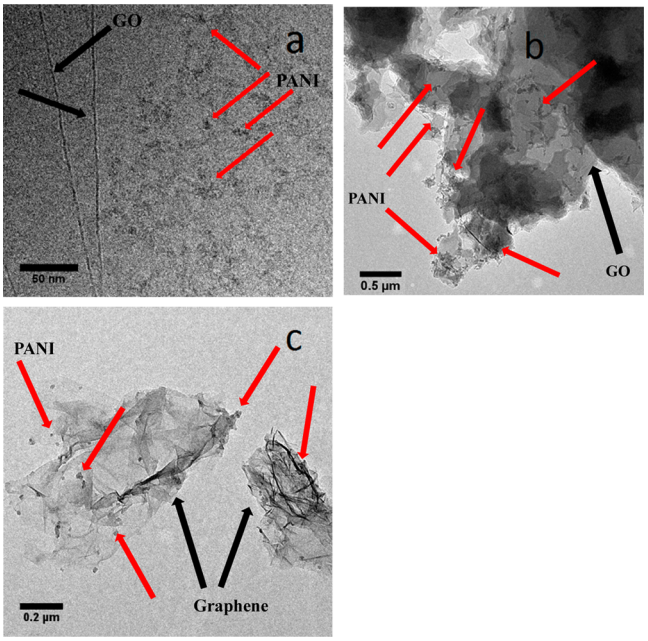

Figure 6. (a) Cryo-TEM image of the mixture solution of GO and PANI. TEM image of (b) freeze-dried GO solution with 2 wt % PANI and (c) graphene/PANI nanocomposites. (Note: In panels a and b, black arrows point to the GO sheets and red arrows point to the PANI particles. In panel c, black arrows point to the graphene sheets and red arrows point to the PANI particles.)

the hydrazine reduction, the PANI nanoparticles were anchored on or sandwiched between the graphene sheets (Figure 6c). It is speculated that, upon mixing GO and PANI in the solution, the PANI nanoparticles tend to adsorb on the GO sheets due to the Coulombic interaction and van der Waals between PANI and GO. When GO is reduced by hydrazine, the hydrophilic functional groups on GO are removed, causing reduced GO sheets to restack. After the hydrazine reduction of the GO, most of the adsorbed PANI nanoparticles were sandwiched between layers of graphene. These PANI nanoparticles act as spacers to create gaps between neighboring graphene sheets, which are accessible by gaseous or liquid species.[36] PANI nanoparticles that are not anchored on the graphene surface may play a role in reducing particle agglomeration during the drying process.[24] This effect of PANI on reducing graphene interlayer stacking is evidenced by the N_2 adsorption adsorption−desorption isotherms and the pore size distribution, shown in Figures 4 and 5. This result is consistent with our previous work using functionalized carbon blacks as the spacer to prevent graphene restacking.[36]

This work points out several important factors that can influence the surface area of graphene composites. First of all, single-layer GO and nanoparticles must be well dispersed in water. In this work, a dilute dispersion of GO and PANI (0.2 mg/mL) was used to prevent significant aggregates.[37] Second, a strong interaction of GO and nanoparticles is required to uniformly incorporate nanoparticles into the graphene network to prevent restacking. For instance, when acetylene black was used as the spacers, most carbon particles were found to exist near the edge of graphene rather than uniformly disperse between graphene layers.[24] Moreover, the nanoparticles are expected to have a relatively low density, as the nanoparticles also contribute to the total weight of the composites. PANI was chosen as candidate spacers due to its several properties, i.e., good dispersion, strong interaction between PANI and GO/graphene, and low density. Last but not least, the freeze-drying technique can partially reduce restacking of graphene.[38] Overall, on the basis of the XPS spectra, N_2 adsorption−desorption isotherms, pore size distribution, SEM, and TEM observations, it can be concluded that our synthesized graphene/PANI composites exhibited a layered structure, separated by PANI nanoparticles. Such a structure with both a high surface area and a proper size distribution may lead to a faster diffusion rate in graphene/PANI composites, which can be utilized in supercapacitor applications.

3.4. Electrochemical Properties. The electrochemical performance of the graphene and graphene/PANI composites was examined by CV, galvanostatic charge/discharge tests, and electrochemical impedance spectroscopy. Figure 7a shows the CV curves of the graphene/2 wt % PANI composites in 1 M H_2SO_4 with various scan rates in the range of −0.2 to 0.8 V vs Ag/AgCl. Although PANI and the residue functional groups on graphene may contribute to some pseudocapacitance, the CV curves of the graphene/PANI composites are relatively rectangular in shape, indicating excellent capacitance behavior.[24,39] The percentage of pseudocapacitance can be estimated by integrating the area of redox peaks and excluding the contribution of double-layer capacitance. It was found out that pseudocapacitance of graphene/PANI composites was about

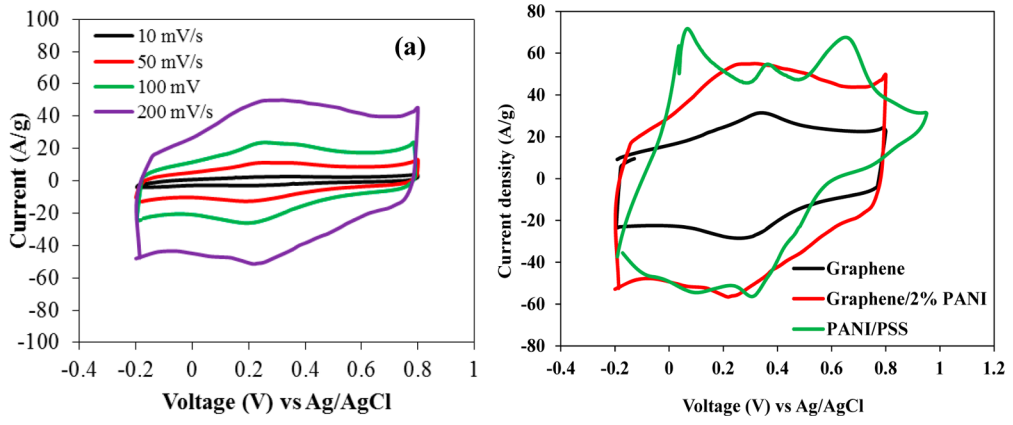

Figure 7. (a) CV curves of graphene/2 wt % PANI nanocomposites at different scan rates of 10, 50, 100, and 200 mV/s in 1 M H_2SO_4 aqueous solution and (b) comparison of CV curves of graphene, PANI, and graphene/2 wt % PANI at 200 mV/s in 1 M H_2SO_4 aqueous solution.

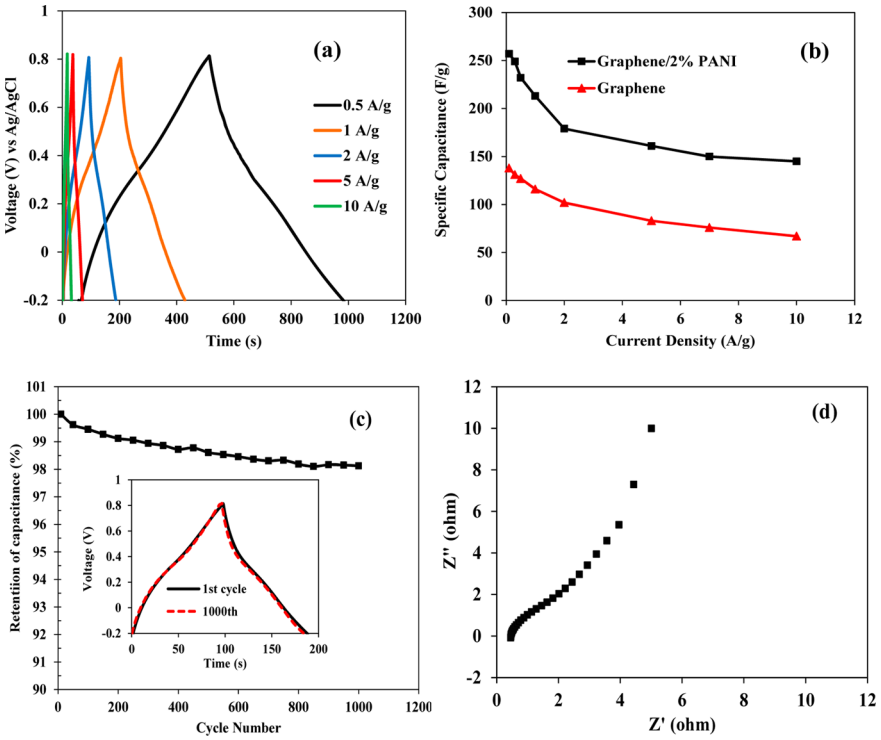

Figure 8. (a) Charge/discharge curves of graphene/2 wt % PANI nanocomposites at current densities of 0.5, 1, 2, 5, and 10 A/g in 1 M H_2SO_4, (b) specific capacitance of graphene and graphene/2 wt % PANI, (c) cycling performance of graphene/2 wt % PANI nanocomposites at 2 A/g in 1 M H_2SO_4 (Inset: charge/discharge curves of 1st and 1000th cycle), and (d) Nyquist plot of of graphene/2 wt % PANI nanocomposites in 1 M H_2SO_4 at open circuit potential with AC amplitude of 5 mV over the frequency range from 100 kHz to 0.1 Hz. Z' is real impedance. Z'' is imaginary impedance.

17% of the total capacitance, which is much higher than that of graphene (6%). Considering there is only a few percent of PANI in the composites, such high percentage of pseudocapacitance may originate from the high capacitance of PANI[40] and synergistic effect between PANI and graphene.[41] At the same scan rate, the larger current response of the graphene/PANI composites means a higher capacitance than that of pure graphene (Figure 7b). The capacitance of a supercapacitor is proportional to the accessible surface area.[42] The larger capacitance of graphene/PANI composites probably results from the higher surface area of graphene/PANI and the enhanced accessibility by electrolyte ions.

The galvanostatic charge/discharge curves of graphene/2 wt % PANI nanocomposites were performed at different current densities (Figure 8a). The specific capacitance of graphene and graphene/2 wt % PANI was calculated on the basis of galvanostatic discharge curves using eq 1 and is shown in Figure 8b. The shape of all charge/discharge curves is nearly linear and symmetric, which is characteristic of a good capacitance. At 0.1 A/g, the specific capacitance of graphene/PANI composites is 257 F/g, and even at 10 A/g, the specific capacitance is 145 F/g. Again, the graphene/PANI composites exhibited a much higher specific capacitance (213 F/g at 1 A/g) than pure graphene (116 F/g at 1 A/g), resulting from the higher surface area of the composites and a faster ion diffusion rate. The capacitances of graphene/PANI composites are higher than those of previously reported graphene,[10,43,44] CNT,[45] and activated carbons.[46,47] The cycling life of graphene/PANI composites was tested at a charge/discharge rate of 2 A/g (Figure 8c). After 1000 cycles, the capacitance still remained about 98% of initial performance. In Figure 8d, the Nyquist plot of the graphene/PANI composites showed an arc shape in the high frequency region and then a vertical line in the low frequency region. The vertical line at low frequency region indicates a good capacitive behavior, representative of fast ion diffusion in the electrode material. The equivalent series resistance (ESR) can be estimated from the x-intercept of the Nyquist plot to be about 0.5 Ω. This low ESR could be attributed to high conductivity of graphene in the composite electrode. Electrochemical measurements have shown that graphene/PANI composites can be a promising candidate material for supercapacitor applications where high surface area and suitable pore size distribution is required.

4. CONCLUSION

Graphene/PANI nanocomposites have been prepared by reducing graphene oxide with hydrazine in the presence of PANI nanoparticles. The incorporation of PANI nanoparticles can effectively reduce the layer-to-layer stacking of graphene. After the reduction is complete, PANI nanoparticles were sandwiched between layers of graphene and acted as spacers to create gaps between neighboring graphene sheets. A high surface area of 891 m^2/g was achieved in graphene/2% PANI (wt % ratio to GO) composites, which is much larger than pure graphene (268 m^2/g). Electrodes made with the nanocomposites exhibited a specific capacitance of 257 F/g at a current density of 0.1 A/g, much higher than that of pure graphene (138 F/g). Even at 10 A/g, the capacitance of the composites was still 145 F/g. Our results have shown that graphene/PANI nanocomposites possess superior electrochemical performance as supercapacitors, mainly due to their

dx.doi.org/10.1021/am4001634 | ACS Appl. Mater. Interfaces 2013, 5, 2685−2691

large surface area and excellent accessibility of mesopores to electrolyte ions.

■ ASSOCIATED CONTENT

Supporting Information

XPS spectra and high resolution C 1s spectra of of the PANI, graphene oxides, graphene, and graphene/PANI composites; SEM image of PANI/PSS nanoparticles; EIS of graphene/PANI composites; table of pore size and pore volume of graphene and graphene/PANI. This material is available free of charge via the Internet at http://pubs.acs.org.

■ AUTHOR INFORMATION

Corresponding Author

*E-mail: jianxie@Iupui.edu.

Notes

The authors declare no competing financial interest.

■ ACKNOWLEDGMENTS

This work was partially supported by the multidisciplinary Undergraduate Research Initiative (MURI) of Indiana University Purdue University Indianapolis (IUPUI). The authors acknowledge Dr. Kateryna Artyushkova for the help in XPS experiments.

■ REFERENCES

(1) Novoselov, K. S.; Geim, A. K.; Morozov, S. V.; Jiang, D.; Zhang, Y.; Dubonos, S. V.; Grigorieva, I. V.; Firsov, A. A. *Science* **2004**, *306*, 666−669.
(2) Allen, M. J.; Tung, V. C.; Kaner, R. B. *Chem. Rev.* **2009**, *110*, 132−145.
(3) Huang, X.; Qi, X.; Boey, F.; Zhang, H. *Chem. Soc. Rev.* **2012**, *41*, 666−686.
(4) Shao, Y.; Wang, J.; Wu, H.; Liu, J.; Aksay, I. A.; Lin, Y. *Electroanalysis* **2010**, *22*, 1027−1036.
(5) Xia, F.; Farmer, D. B.; Lin, Y.-m.; Avouris, P. *Nano Lett.* **2010**, *10*, 715−718.
(6) Huang, B.; Li, Z.; Liu, Z.; Zhou, G.; Hao, S.; Wu, J.; Gu, B.-L.; Duan, W. *J. Phys. Chem. C* **2008**, *112*, 13442−13446.
(7) Shang, N.; Papakonstantinou, P.; Wang, P.; Silva, S. R. P. *J. Phys. Chem. C* **2010**, *114*, 15837−15841.
(8) Guo, P.; Song, H.; Chen, X. *Electrochem. Commun.* **2009**, *11*, 1320−1324.
(9) Zhou, X.; Wang, F.; Zhu, Y.; Liu, Z. *J. Mater. Chem.* **2011**, *21*, 3353.
(10) Stoller, M. D.; Park, S.; Zhu, Y.; An, J.; Ruoff, R. S. *Nano Lett.* **2008**, *8*, 3498−3502.
(11) Liu, C.; Yu, Z.; Neff, D.; Zhamu, A.; Jang, B. Z. *Nano Lett.* **2010**, *10*, 4863−4868.
(12) Zhang, L.; Shi, G. *J. Phys. Chem. C* **2011**, *115*, 17206−17212.
(13) Hulman, M.; Haluška, M.; Scalia, G.; Obergfell, D.; Roth, S. *Nano Lett.* **2008**, *8*, 3594−3597.
(14) Yang, X.; Dou, X.; Rouhanipour, A.; Zhi, L.; Räder, H. J.; Müllen, K. *J. Am. Chem. Soc.* **2008**, *130*, 4216−4217.
(15) Berger, C.; Song, Z.; Li, T.; Li, X.; Ogbazghi, A. Y.; Feng, R.; Dai, Z.; Marchenkov, A. N.; Conrad, E. H.; First, P. N.; de Heer, W. A. *J. Phys. Chem. B* **2004**, *108*, 19912−19916.
(16) Li, X.; Cai, W.; An, J.; Kim, S.; Nah, J.; Yang, D.; Piner, R.; Velamakanni, A.; Jung, I.; Tutuc, E.; Banerjee, S. K.; Colombo, L.; Ruoff, R. S. *Science* **2009**, *324*, 1312−1314.
(17) Kim, K. S.; Zhao, Y.; Jang, H.; Lee, S. Y.; Kim, J. M.; Kim, K. S.; Ahn, J.-H.; Kim, P.; Choi, J.-Y.; Hong, B. H. *Nature* **2009**, *457*, 706−710.
(18) Gilje, S.; Han, S.; Wang, M.; Wang, K. L.; Kaner, R. B. *Nano Lett.* **2007**, *7*, 3394−3398.
(19) Gómez-Navarro, C.; Weitz, R. T.; Bittner, A. M.; Scolari, M.; Mews, A.; Burghard, M.; Kern, K. *Nano Lett.* **2007**, *7*, 3499−3503.
(20) Yoo, E.; Kim, J.; Hosono, E.; Zhou, H.-s.; Kudo, T.; Honma, I. *Nano Lett.* **2008**, *8*, 2277−2282.
(21) Zhu, Y.; Murali, S.; Cai, W.; Li, X.; Suk, J. W.; Potts, J. R.; Ruoff, R. S. *Adv. Mater.* **2010**, *22*, 3906−3924.
(22) Wu, Z.-S.; Wang, D.-W.; Ren, W.; Zhao, J.; Zhou, G.; Li, F.; Cheng, H.-M. *Adv. Funct. Mater.* **2010**, *20*, 3595−3602.
(23) Si, Y.; Samulski, E. T. *Chem. Mater.* **2008**, *20*, 6792−6797.
(24) Yan, J.; Wei, T.; Shao, B.; Ma, F.; Fan, Z.; Zhang, M.; Zheng, C.; Shang, Y.; Qian, W.; Wei, F. *Carbon* **2010**, *48*, 1731−1737.
(25) Hummers, W. S.; Offeman, R. E. *J. Am. Chem. Soc.* **1958**, *80*, 1339−1339.
(26) Kovtyukhova, N. I.; Ollivier, P. J.; Martin, B. R.; Mallouk, T. E.; Chizhik, S. A.; Buzaneva, E. V.; Gorchinskiy, A. D. *Chem. Mater.* **1999**, *11*, 771−778.
(27) Jang, J.; Ha, J.; Cho, J. *Adv. Mater.* **2007**, *19*, 1772−1775.
(28) Stankovich, S.; Dikin, D. A.; Piner, R. D.; Kohlhaas, K. A.; Kleinhammes, A.; Jia, Y.; Wu, Y.; Nguyen, S. T.; Ruoff, R. S. *Carbon* **2007**, *45*, 1558−1565.
(29) Park, S.; An, J.; Potts, J. R.; Velamakanni, A.; Murali, S.; Ruoff, R. S. *Carbon* **2011**, *49*, 3019−3023.
(30) Compton, O. C.; Jain, B.; Dikin, D. A.; Abouimrane, A.; Amine, K.; Nguyen, S. T. *ACS Nano* **2011**, *5*, 4380−4391.
(31) Yang, D.; Velamakanni, A.; Bozoklu, G.; Park, S.; Stoller, M.; Piner, R. D.; Stankovich, S.; Jung, I.; Field, D. A.; Ventrice, C. A., Jr.; Ruoff, R. S. *Carbon* **2009**, *47*, 145−152.
(32) Sing, K. S. W.; Everett, D. H.; Haul, R. A. W.; Moscou, L.; Pierotti, R. A.; Rouquerol, J.; Siemieniewska, T. *Pure Appl. Chem.* **1985**, *57*, 603−619.
(33) Li, N.; Liu, G.; Zhen, C.; Li, F.; Zhang, L.; Cheng, H.-M. *Adv. Funct. Mater.* **2011**, *21*, 1717−1722.
(34) Zhu, Y.; Murali, S.; Stoller, M. D.; Ganesh, K. J.; Cai, W.; Ferreira, P. J.; Pirkle, A.; Wallace, R. M.; Cychosz, K. A.; Thommes, M.; Su, D.; Stach, E. A.; Ruoff, R. S. *Science* **2011**, *332*, 1537−1541.
(35) Yoo, S. J.; Cho, J.; Lim, J. W.; Park, S. H.; Jang, J.; Sung, Y.-E. *Electrochem. Commun.* **2010**, *12*, 164−167.
(36) Wang, M.-x.; Liu, Q.; Sun, H.-f.; Stach, E. A.; Zhang, H.; Stanciu, L.; Xie, J. *Carbon* **2012**, *50*, 3845−3853.
(37) Chiou, N. R.; Epstein, A. J. *Adv. Mater.* **2005**, *17*, 1679−1683.
(38) Korkut, S.; Roy-Mayhew, J. D.; Dabbs, D. M.; Milius, D. L.; Aksay, I. A. *ACS Nano* **2011**, *5*, 5214−5222.
(39) Numao, S.; Judai, K.; Nishijo, J.; Mizuuchi, K.; Nishi, N. *Carbon* **2009**, *47*, 306−312.
(40) Li, H.; Wang, J.; Chu, Q.; Wang, Z.; Zhang, F.; Wang, S. *J. Power Sources* **2009**, *190*, 578−586.
(41) Xu, J.; Wang, K.; Zu, S.-Z.; Han, B.-H.; Wei, Z. *ACS Nano* **2010**, *4*, 5019−5026.
(42) Pandolfo, A. G.; Hollenkamp, A. F. *J. Power Sources* **2006**, *157*, 11−27.
(43) Wang, Y.; Shi, Z.; Huang, Y.; Ma, Y.; Wang, C.; Chen, M.; Chen, Y. *J. Phys. Chem. C* **2009**, *113*, 13103−13107.
(44) Zhang, K.; Mao, L.; Zhang, L. L.; On Chan, H. S.; Zhao, X. S.; Wu, J. *J. Mater. Chem.* **2011**, *21*, 7302−7307.
(45) Kaempgen, M.; Chan, C. K.; Ma, J.; Cui, Y.; Gruner, G. *Nano Lett.* **2009**, *9*, 1872−1876.
(46) Gamby, J.; Taberna, P. L.; Simon, P.; Fauvarque, J. F.; Chesneau, M. *J. Power Sources* **2001**, *101*, 109−116.
(47) Fernández, J. A.; Morishita, T.; Toyoda, M.; Inagaki, M.; Stoeckli, F.; Centeno, T. A. *J. Power Sources* **2008**, *175*, 675−679.